energies

MDPI

Article

The Effect of Electro–Thermal Ageing of Polymer–Ceramic Nanocomposite Insulation on Dielectric Endurance

Keyvan Rasti [1,2], Sathyamoorthy Dhayalan [1,2], Nick Tucker [1], Len Dissado [3] and Nikola Chalashkanov [1,*]

[1] School of Engineering and Physical Sciences, University of Lincoln, Lincoln LN6 7TS, UK; 26337771@students.lincoln.ac.uk (K.R.); sathyamoorthy.dhayalan@gmail.com (S.D.); ntucker@lincoln.ac.uk (N.T.)
[2] DPI Netherlands (Dutch Polymer Institute), P.O. Box 902, 5600 AX Eindhoven, The Netherlands
[3] School of Engineering, University of Leicester, Leicester LE1 7RH, UK; lad4@leicester.ac.uk
* Correspondence: nchalashkanov@lincoln.ac.uk

Abstract

This study investigates the electro-thermal ageing (ETA) behaviour of neat polyamide-6 (PA6) and PA6/barium titanate (BTO) nanocomposites. Time–to–breakdown measurements were performed at 333 K, 353 K, and 373 K at field strengths between 50 and 90 kV/mm to assess the impact of nanofiller level on lifetime to failure. The ageing experiment showed that moderate amounts of nanofiller improved the electro-thermal endurance while excessive filler addition (20 wt.%) led to faster breakdown. The Dissado–Montanari–Mazzanti (DMM) model was used to evaluate the ageing parameters for neat PA6 and PA6/10 wt.% BTO across all three temperatures. Neat PA6 and PA6/10 wt.% BTO both showed nearly identical activation enthalpy (H/k) values, indicating that the intrinsic thermally activated ageing mechanism of PA6 is preserved in the nanocomposite. Variations in the field-sensitivity parameters (C/k and b) align with an interpretation involving changes in charge transport and interfacial trapping introduced by the addition of BTO. Furthermore, analysis of all filler concentrations confirmed that 1–10 wt.% BTO maintains or slightly improves the time to breakdown, while 20 wt.% significantly accelerated the ageing process. This research forms part of the research programme of DPI, project #852.

Keywords: electrothermal ageing; life estimation; polymer-ceramic nanocomposite; DMM model

1. Introduction

Insulation materials have very high electric-field breakdown strength and low conductivity to prevent current leakage between electrodes of different potential and to ensure safe and stable operation of the power equipment. Polymer–ceramic nanocomposites are highly promising candidates for next-generation high-voltage insulation materials [1–4]. Their engineered microstructures deliver enhanced breakdown strength, higher permittivity, and improved resistance to surface discharge when compared with conventional polymer composites; there is variation related to filler type and concentration [5,6]. These advantages are exploited in diverse applications, including power transmission cable insulation [2] and energy storage systems such as capacitors and lithium-ion batteries [6–8]. Nanocomposites containing ceramic fillers have been recognised as effective for capacitive energy storage due to their combination of high permittivity and superior breakdown performance since the energy storage density of dielectric materials is proportional to the permittivity and the square of the breakdown field [3,6–8]. Barium titanate (BTO) is widely used as a ceramic

Check for updates

Academic Editor: Mario Marchesoni

Received: 24 February 2026
Revised: 18 March 2026
Accepted: 20 March 2026
Published: 26 March 2026

Copyright: © 2026 by the authors. Licensee MDPI, Basel, Switzerland. This article is an open access article distributed under the terms and conditions of the Creative Commons Attribution (CC BY) license.

filler in polymer nanocomposites [9] due to its superior ferroelectric, piezoelectric, and dielectric characteristics. In silicone rubber–BTO nanocomposites, commonly used for outdoor insulation, it has been shown to improve resistance to degradation processes such as erosion and tracking, thereby enhancing overall insulation performance [10]. Among candidate polymer matrices, polyamide-6 (PA6) is a semi-crystalline polymer widely used in electrical insulation due to its favourable mechanical strength, thermal stability, and ease of processing. It also exhibits moderate dielectric strength and relatively low dielectric loss, making it suitable for high-voltage applications [11].

To date, much research has focused on improving short-term dielectric properties, with relatively less attention given to the long–term reliability of nanocomposite insulation under service conditions. The service conditions include wide range of temperatures, pressures and electric fields depending on the application. In practical applications such as capacitors, insulation materials are continuously exposed to electro-thermal stress [12], which accelerates ageing and degradation, ultimately leading to electrical failure. Ageing can be described as the process that alters the physical or chemical state of the material, while degradation refers specifically to changes that impair performance—most critically, the dielectric breakdown strength [13]. Failures observed at low fields and short times are often attributed to localised degradation [13,14] rather than bulk deterioration. Previous studies have linked ageing-induced increases in AC dielectric loss to changes at the interface between the metal electrode and the insulation material, which in turn correlate with reduced breakdown strength [15]. However, reported changes in DC conductivity with ageing remain inconsistent across materials [14,15]. Comparable observations have been made in fibre-reinforced epoxy systems, where AC dielectric changes were associated with microcracking [4] and delamination [16]. These localised degradations may arise from electrically driven weakening of the polymer–filler interface, eventually causing local mechanical yielding [17,18]. The lifetime, ageing mechanisms, and breakdown phenomena in nanocomposite dielectrics may differ significantly from those in unfilled polymers due to nanofiller type, size, concentration, and surface functionalization. Therefore, the understanding and prediction of insulation lifetime under such conditions is both important and challenging [13,19]. Systematic experimental studies to clarify electro-thermal ageing behaviour with different levels of nanofiller and to establish robust lifetime prediction methods are therefore required.

The present work addresses this gap by experimentally investigating the electrothermal ageing of PA6 and PA6/$BaTiO_3$ (BTO) nanocomposites. The effect of nanofiller content (0–20 wt.%) was studied at two temperatures (353 K and 373 K) under electric fields ranging from 60 to 90 kV/mm. In addition, a comparison between neat PA6 and PA6/10 wt.% BTO nanocomposites was performed over three temperatures (333 K, 353 K, and 373 K) and five electric-field levels (50–90 kV/mm). The lifetimes derived from time–to–breakdown measurements are analysed using the Dissado–Montanari–Mazzanti (DMM) life model and compared to the long-term performance of the neat polymer. The aim is to compare the ageing behaviour of neat polymers and nanocomposites in order to provide an insight into the role of nanofiller concentration in enhancing long-term dielectric reliability.

2. DMM Model

Several empirical and semi-empirical models have previously been used to predict the lifetime of polymeric insulation under electrical and thermal stress, including Arrhenius thermal ageing, the Inverse Power Law (IPL), exponential voltage–endurance models, and phenomenological multi-stress formulations [20]. Although these approaches are simple to implement, they suffer from a fundamental limitation: they treat electrical and thermal stresses as independent or additively combined, despite clear evidence that real insulation

degradation is governed by coactive and strongly nonlinear interactions between multiple stressors. Their fitting parameters lack physical meaning, as they do not account for charge injection or space-charge-induced field enhancement [21].

In contrast, the Dissado–Montanari–Mazzanti (DMM) model provides a fundamentally grounded physics-based description of electro-thermal ageing by representing the polymer as a system of molecular units undergoing a thermally activated degradation process whose activation barrier is lowered by the applied electric field through charge trapping and local field intensification. The DMM parameters—activation enthalpy, field-acceleration coefficient, and field exponent—are directly linked to material behaviour and microstructural features. As a result, the DMM model captures curvature in lifetime–field plots, predicts electrical and thermal threshold effects, and identifies the onset of irreversible degradation rather than only final breakdown. These features make the DMM framework significantly more robust, interpretable, and reliable than traditional empirical methods for modelling the long-term electro-thermal performance of polymeric insulation [21].

Electro-thermal ageing in polymeric insulation is understood as a progressive accumulation of irreversible chemical and structural changes within the material. In the DMM framework, the polymer is modelled as an ensemble of local molecular units that can exist in two inter-convertible states: an unaged (reactant) state and a degraded (product) state. Ageing proceeds through a thermally activated reversable reaction mechanism between these states, with the applied electric field lowering the effective energy barrier for the transition [22]. When the fraction of degraded units within a local region reaches a critical threshold, electrical breakdown initiates [23,24]. This microscopic description of ageing leads directly to a physical electro-thermal lifetime expression that relates the time to failure of the insulation to the applied electric field and temperature, expressed by the DMM life model in Equation (1) [25]:

$$L = \left(\frac{h}{2kT}\right)\exp\left(\frac{H}{kT}\right)\exp\left(-\frac{CE^b}{2kT}\right)\left[\frac{-\ln\left[\frac{\left(A_{eq}-A^*\right)}{A_{eq}}\right]}{\cosh\left(\frac{\Delta-CE^b}{2kT}\right)}\right], \quad (1)$$

Here h is Planck's constant, k is Boltzmann's constant. E is the electric field (kV/mm), and T is the absolute temperature (K), The parameters H/k, C/k, and b are the model's characteristic ageing coefficients, corresponding to the activation enthalpy, a field-acceleration term, and a field-dependence exponent, respectively. A^* is the critical degradation threshold at which breakdown occurs, and the quantity A_{eq} denotes the equilibrium degraded fraction which is defined by Equation (2):

$$A_{eq} = \frac{1}{\left[1+\exp\left(\frac{\Delta-CE^b}{kT}\right)\right]}, \quad (2)$$

Here, Δ is the energy difference between the reacted and unreacted states. In the limited field range of the current data, Δ has little effect, and we will take it to be zero for simplicity. When the reaction process reaches the critical value of A^*, runaway breakdown occurs. Here, A^* is taken to be approximately 0.43, as suggested by previous studies on thin polymer samples [25].

3. Materials and Methods

3.1. Sample Preparation

The samples were prepared by melt compounding polyamide-6 (PA6) with barium titanate (BTO) nanoparticles using a twin-screw extrusion process. PA6 (Akulon K122,

Envalior) was used as the base polymer, while barium titanate nanoparticles (BTO, Nanostructured & Amorphous Materials Inc., Katy, TX, USA) were used as the nanofiller. The PA6 pellets and BTO nano powder were fed into a twin-screw compounding extruder through separate gravimetric feeders to ensure accurate formulation and homogeneous mixing. Following compounding, the extrudate was cooled in a water bath and subsequently pelletised to produce uniformly sized PA6/BTO nanocomposite pellets. Prior to sample fabrication, the pellets were dried in a vacuum oven at 353 K for 24 h to remove residual moisture. After drying, the pellets were processed by extrusion to produce thin films. The extrusion was carried out at a screw speed of approximately 30 rpm, with processing temperatures maintained around 513 K (above the melting temperature of PA6) along the extrusion barrel. Thin films used for the electrothermal ageing experiments were then prepared from the dried pellets, resulting in samples with a nominal thickness of approximately 50 µm. The PA6/BTO nanocomposite materials were manufactured by Envalior (Eindhoven, The Netherlands). The thickness of the samples prepared for the electrothermal experiments was nominally 50 µm and the BTO particle size was between 100 and 200 nm. The morphology and dispersion of BTO nanoparticles within the PA6 matrix were examined using scanning electron microscopy (SEM) equipped with an energy-dispersive X-ray spectroscopy (EDX) detector (Bruker XFlash 6-60, Billerica, MA, USA). The observations were carried out at an accelerating voltage of 5 kV. As shown in Figure 1, the BTO nanoparticles are relatively uniformly dispersed within the PA6 matrix, which is consistent with previous report [26]. The nanocomposite sample filler contents are listed in Table 1.

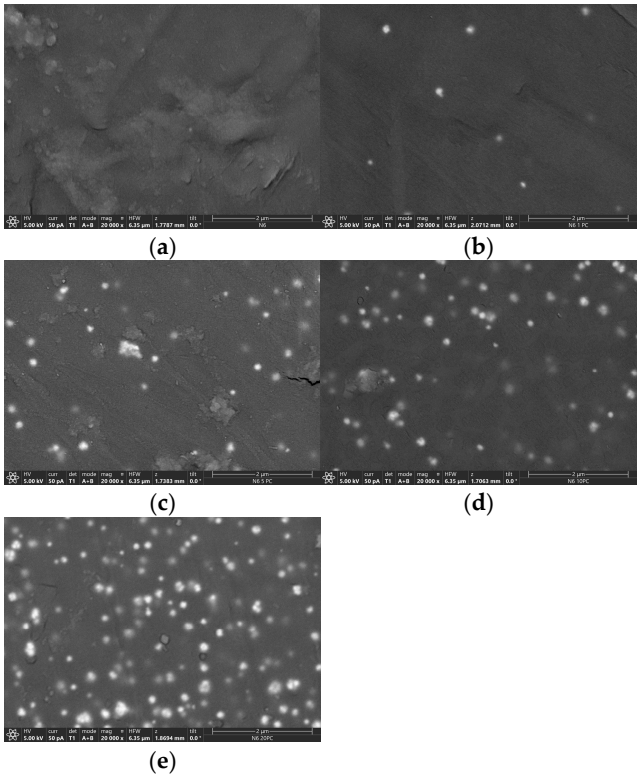


Figure 1. SEM images (20,000× magnification) show the dispersion of BTO nanoparticles in PA6 nanocomposites: (**a**) neat PA6, (**b**) PA6/1 wt.% BTO, (**c**) PA6/5 wt.% BTO, (**d**) PA6/10 wt.% BTO, and (**e**) PA6/20 wt.% BTO. The bright regions correspond to BTO nanoparticles dispersed within the PA6 matrix.

Table 1. Polymer–ceramic (PA6-BTO) nanocomposite details.

Sample	Sample Formulation
1	Neat PA6
2	PA6/1 wt.% BTO
3	PA6/5 wt.% BTO
4	PA6/10 wt.% BTO
5	PA6/20 wt.% BTO

3.2. Electro-Thermal Ageing Experimental Setup

To investigate the combined influence of electrical and thermal stress, the experimental configuration, illustrated in Figure 2 was employed. A Genlab laboratory oven provided controlled thermal stress, while a test cell equipped with eight cylindrical brass electrodes served as the high-voltage (HV) chamber. The electrodes were connected to a 100 kV DC power supply (Glassman 100 kV, 3 mA), with the brass electrodes functioning as the HV terminals and an aluminium plate as the grounded electrode. The high-voltage electrodes, designed in accordance with IEC 60243, had a diameter of 2 cm and a 3 mm edge curvature to eliminate sharp edges that could otherwise cause local field enhancement and premature breakdown. The electrode surfaces were polished with 1 µm diamond paste to ensure a uniform electric field across the specimen. The top electrodes were connected to the HV source through a current limiting safety resistor, whilst the bottom electrode was grounded. Test samples were positioned between the electrodes, and the entire assembly was immersed in silicone oil to prevent surface flashover between the terminals.

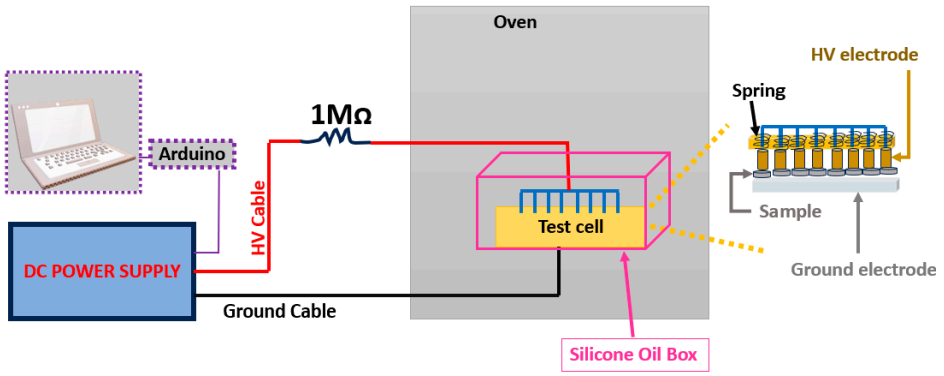


Figure 2. Schematic of electro-thermal experimental test setup to detect the time to breakdown of the test.

A MATLAB-based data-acquisition programme (MATLAB R2019b, MathWorks, Natick, MA, USA) interfaced with an Arduino Uno Rev3 board was developed to automatically record the time to breakdown of each sample. Breakdown events were detected by the Arduino, which immediately reduced the applied voltage to zero and stored the breakdown time on a connected PC. The DC voltage was ramped at a constant rate of 200 V/s until the target field was reached, after which it was held constant until breakdown occurred. Both the applied voltage and the corresponding electric field were continuously monitored via the Arduino interface. The oven temperature was tracked using a thermocouple to ensure stable thermal conditions. Prior to testing, all samples were pre-dried in a vacuum oven at 348 K for 15 h to remove moisture. Electro-thermal ageing tests were conducted at five DC electric–field levels (50–90 kV/mm) and three temperatures (333 K, 353 K, and 373 K). For each electric–field level and nanofiller concentration, eight samples were tested, as illustrated in Figure 2. However, due to the time-consuming nature of the ETA experiments,

the effect of nanofiller concentration was evaluated using the experimental data obtained at 353 K and 373 K across the same range of electric–field levels.

4. Results

4.1. Electro-Thermal Ageing Results

Figure 3 shows the time to breakdown of neat PA6 and PA6/BTO nanocomposites under DC fields at three temperatures. From Figure 3 and the quantitative comparison summarised in Table 2, at high electric-field strengths (70–90 kV/mm), the addition of nanofillers has little influence on breakdown behaviour at 333 K and 353 K. The only exception is the data obtained at 373 K, where the lifetime of the nanocomposites is significantly lower than the neat polymer, with reductions reaching approximately 60% at 80–90 kV/mm, as reported in Table 2. This suggests that under high electrical stress, the breakdown is dominated by the intrinsic dielectric strength of the polymer. Overall, the high-field results indicate that the addition of BTO generally reduces the lifetime relative to neat PA6 at 333 K and 373 K, while only a slight lifetime increase (less than 15%) is observed at 353 K. In contrast, at lower electric fields (<70 kV/mm), the role of nanofillers becomes more evident. As shown in Figure 3 and Table 2, PA6 containing 10 wt.% BTO, representative of polymer–ceramic nanocomposites, exhibits a substantially longer time to breakdown than neat PA6 at the lowest applied electric field. Lifetime improvements of approximately 30–50% are observed at 333–353 K, increasing to more than 70% at 373 K under an applied electric field of 60 kV/mm, suggesting an enhanced resistance to degradation.

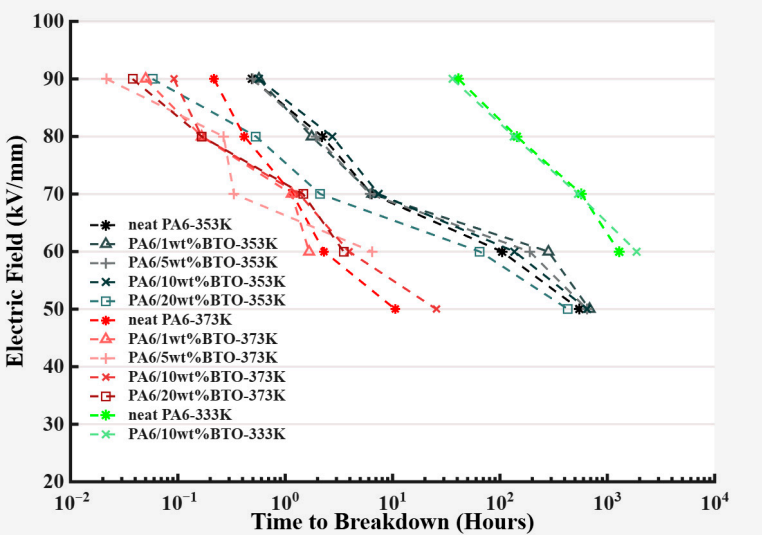


Figure 3. Time to breakdown of neat PA6 and PA6/BTO nanocomposites under DC electric fields at different temperatures.

All samples demonstrated a reduced lifetime at 373 K, confirming that elevated temperatures accelerate ageing processes. This behaviour is consistent with thermally activated degradation, in which higher temperature increases the probability that reactant units overcome the activation barrier, thereby accelerating the chemical and physical ageing reactions. At 353 K and 373 K, however, the nanocomposite with 20 wt.% BTO displayed a shorter lifetime than neat PA6. This suggests that excessive filler loading may induce filler agglomeration [27] or interfacial defects [28,29], which act as weak points under combined electrical and thermal stress. In such cases, the presence of a high concentration of nanofillers may actually facilitate degradation (due to the introduction of weak points in the insulation) rather than improve ageing resistance, which can be confirmed by the data extraction from the DMM model.

Table 2. Relative change in time to breakdown (%) for PA6/10 wt.% BTO compared with neat PA6 at electric fields between 60 and 90 kV/mm and temperatures of 333 K, 353 K, and 373 K.

T (K)	E (kV/mm)	% Change in the Time to Breakdown Between PA6/10BTO and Neat PA6
333	90	−12.0
	80	−17.6
	70	−10.6
	60	+46.8
353	90	+10.4
	80	+15.6
	70	−23.3
	60	+31.0
373	90	−57.7
	80	−60.0
	70	+15.7
	60	+70.8

4.2. Life Estimation of Neat Polymer and Nanocomposite

The lifetime behaviour of neat PA6 and PA6/10 wt.% BTO nanocomposites was analysed using the Dissado–Montanari–Mazzanti (DMM) life model. The model parameters—H/k, C/k, and b—were obtained by fitting the experimental time-to-breakdown data across the 50–90 kV/mm field range at three test temperatures. The combined experimental data and DMM fits are shown in Figure 4.

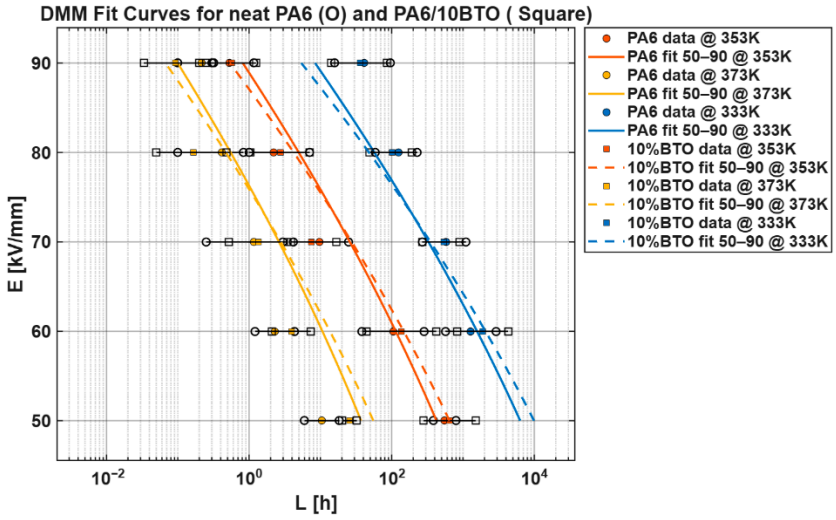


Figure 4. Experimental lifetime data with 95% confidence limits (markers) and Dissado–Montanari –Mazzanti (DMM) model fitting for neat PA6 (solid lines) and PA6/10BTO (dashed lines).

According to the extracted parameters summarised in Table 3, both materials display very similar ageing characteristics, with $\frac{H}{k} \approx (1.69 - 1.72) \times 10^4$ K, $\frac{C}{k} \approx 1.36 - 1.34$, and $b \approx 1.74 - 1.77$. The closeness of the parameter values and the similarity of the fitted lines indicate that the incorporation of BTO nanofillers does not fundamentally alter the ageing mechanism but does slightly modify the strength of the electric-field influence on the ageing process. Importantly, comparison of the fitted curves with the experimental data for these two representative systems—polymer (PA6) and polymer–ceramic nanocomposite (PA6/10BTO)—reveals a clear field-dependent effect. In the high-field regime (70–90 kV/mm), the addition of BTO results in a reduced lifetime compared to neat PA6, whereas at lower electric fields (<70 kV/mm) the PA6/10BTO system exhibits an

increased lifetime. This behaviour is consistent with the trends reported in Table 2 and can be attributed to the slight reduction in C/k from 1.36 for neat PA6 to 1.34 for PA6/10BTO. The influence of this parameter change on the fitted lifetime curves are further examined through a sensitivity analysis, which is discussed following the detailed assessment of nanofiller effects on the electro-thermal ageing (ETA) behaviour.

Table 3. Extracted DMM model fitting parameters (H/k), (C/k), and b for neat PA6 and PA6/10 wt.% BTO over the electric field range of 50–90 kV/mm, samples at 333 K, 353 K and 373 K.

Sample ID	(H/k) K	(C/k) K(kV/mm)$^{-b}$	b
Neat PA6	1.692×10^4	1.362	1.74
PA6/10 wt.% BTO	1.72×10^4	1.344	1.77

To examine the influence of barium titanate (BTO) nanofiller concentration on the electro-thermal ageing behaviour of PA6/BTO nanocomposites, the DMM model was fitted to the experimental data. The fitting was performed (see Table 1 for materials used) as shown in Figures 5 and 6, using experimental lifetime data obtained at two temperatures, 353 K over the 50–90 kV/mm field range and 373 K over the 60–90 kV/mm range. The model parameters are extracted for each composition, and the results are summarised in Table 4.

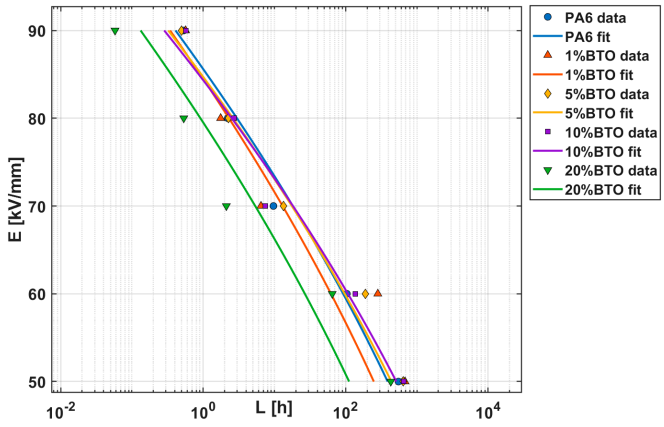


Figure 5. Experimental lifetime data and DMM model fitting for neat PA6 and PA6/BTO nanocomposites at 353 K.

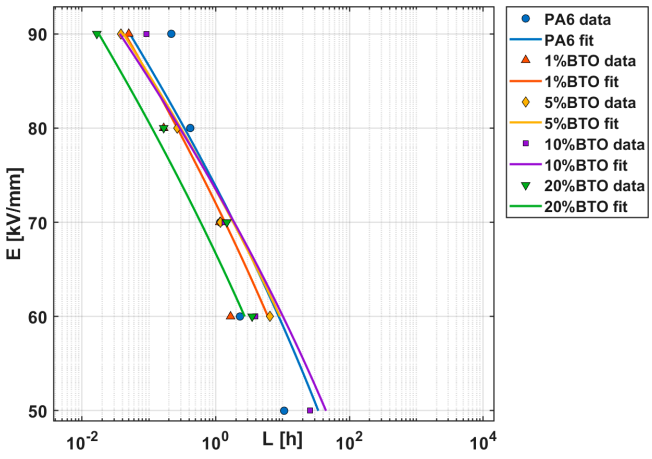


Figure 6. Experimental lifetime data and DMM model fitting for neat PA6 and PA6/BTO nanocomposites at 373 K.

Table 4. Extracted DMM model fitting parameters (H/k), (C/k), and b for all samples at 353 K and 373 K.

Sample ID	(H/k) K	(C/k) K (kV/mm)$^{-b}$	b
Neat PA6	1.70×10^4	1.4311	1.750
PA6/1 wt.% BTO	1.68×10^4	1.4421	1.740
PA6/5 wt.% BTO	1.71×10^4	1.4348	1.760
PA6/10 wt.% BTO	1.72×10^4	1.4222	1.770
PA6/20 wt.% BTO	1.66×10^4	1.7914	1.700

In all cases, the activation enthalpy (H/k) changed between 1.66×10^4 K and 1.72×10^4 K. Similarly, the electric field-related parameters C/k and b exhibited small variations with filler concentration. At low and moderate loadings (1–10 wt.%), both C/k and b values remained close to 1.4 and 1.75, respectively, indicating similar field-dependent ageing characteristics to those of the neat polymer.

At a higher loading (20 wt.% BTO), C/k increased to 1.79, while b slightly decreased to 1.70, indicating a stronger field sensitivity and a reduction in the nonlinearity of the field dependence.

To clarify the physical significance of the DMM parameters, a sensitivity analysis was performed by independently varying each parameter, while keeping the remaining parameters fixed at their average values calculated from the data in Table 4. Variations in the activation enthalpy H/k, as shown in Figure 7, primarily result in an approximately parallel shift in the lifetime–electric field curves, indicating that H/k governs the intrinsic thermal timescale of the ageing process.

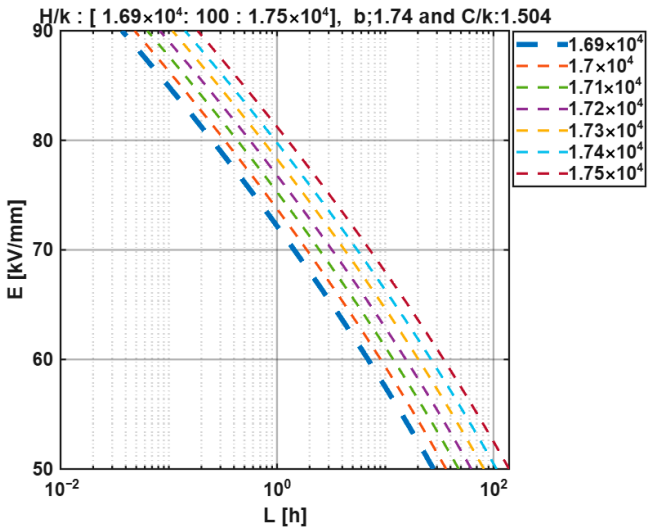


Figure 7. Effect of activation enthalpy H/k on the DMM model.

In contrast, changes in the field-sensitivity parameter C/k, illustrated in Figure 8, significantly modify the curvature of the fitted curves, particularly at high electric fields. Increasing C/k from 1.504 to 1.804, while keeping the other model parameters constant, results in a reduction in lifetime across all electric-field levels. This effect is more pronounced at higher fields (70–90 kV/mm), where the lifetime decreases by approximately 80%, compared to a reduction of about 50% at lower fields (50–60 kV/mm). Similarly, variations in the field exponent b, shown in Figure 9, strongly affect the slope of the lifetime in the high-field regime, highlighting its influence on the nonlinearity of field-driven ageing.

Increasing b from 1.74 to 1.80, while keeping the other parameters constant, significantly accelerates electrical ageing, resulting in a substantial reduction in lifetime across all electric-field levels. This effect is most pronounced at higher fields (70–90 kV/mm), where the lifetime decreases by more than 90%. Taken together, this sensitivity analysis explains why relatively small variations in C/k and b, as observed in Tables 3 and 4, can lead to pronounced differences in lifetime behaviour. The PA6/10 wt.% BTO composite has the lowest value of C/k and the highest value of H/k from all samples; hence, it shows the longest life at applied electric fields below 70 kV/mm. The slightly higher value of the exponent b means that the trend is reversed, and the PA6/10 wt.% BTO composite shows reduced life at the highest applied fields in comparison with neat PA6. The results suggest that the presence of nanofillers primarily modifies the strength and field dependence of the ageing process.

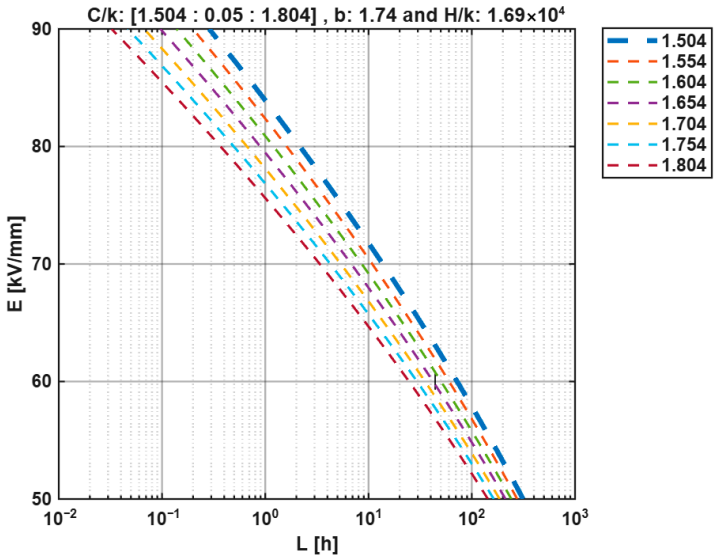


Figure 8. Effect of the field-sensitivity parameter C/k on the DMM model.

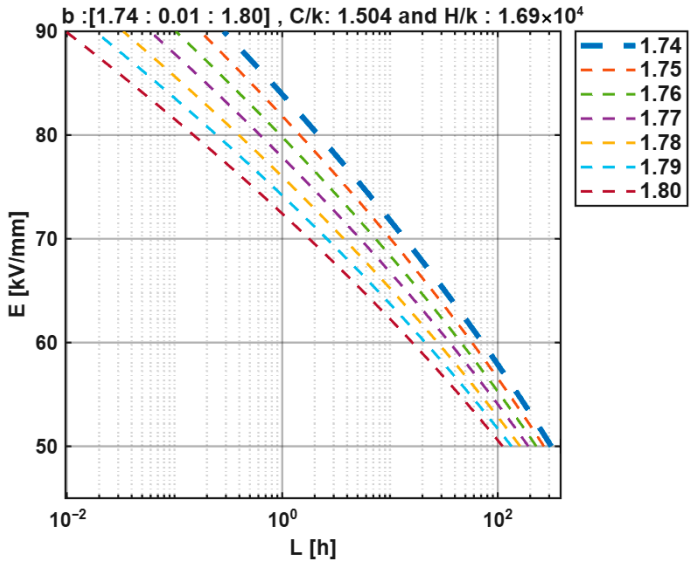


Figure 9. Effect of the field exponent b on the nonlinearity of the DMM model.

5. Discussion

The combined experimental and modelling results provide a comprehensive understanding of the electro-thermal ageing behaviour of neat PA6 and PA6/BTO nanocom-

posites. The experimental data demonstrated clear reductions in lifetime with increasing temperature across all materials, confirming that thermal activation accelerates chemical degradation [30] and microstructural change within the polymer matrix [31,32]. At high electric fields (70–90 kV/mm), the lifetime differences between neat PA6 and the nanocomposites were minimal, suggesting that breakdown in this region is governed predominantly by intrinsic electric field-driven failure [26]. Under such strong fields, rapid charge injection, localised field intensification, and avalanche-like carrier multiplication dominate the failure process, minimising the influence of microstructural modifications introduced by nanofillers [33].

A closer examination of the high-field region highlights a clear temperature-dependent reversal in performance, as summarised in Table 2. At 373 K and electric fields of 80–90 kV/mm, the PA6/10 wt.% BTO nanocomposite exhibits a noticeably shorter time to breakdown than neat PA6, with the lifetime reduced by approximately 60%, as shown in Table 2, indicating that under extreme electrical and thermal stress the presence of ceramic nanoparticles can accelerate degradation rather than delay it. At an elevated temperature, charge transport and charge injection processes become more active, while the strong permittivity mismatch between BTO particles and the polymer matrix promotes interfacial (Maxwell–Wagner) polarisation and pronounced local electric-field concentration at polymer–particle interfaces, analogous to the interface-controlled field localisation reported for BTO-based dielectrics under DC stress [34]. Studies on other titanate ceramics have shown that such localised field enhancement occurs at internal barrier regions and governs degradation at high electric fields, as the effective local field can greatly exceed the applied macroscopic field [35]. Direct experimental evidence from single-crystal titanates further demonstrates that defect redistribution under combined electric field and temperature leads to highly non-uniform field profiles and local field maxima that dominate leakage current growth and degradation kinetics [34]. These local field enhancements are known to promote non-ohmic (Schottky-type) conduction, increased leakage current, and accelerated failure at high fields and temperatures, as established in classical BTO capacitor failure studies [36]. In contrast, neat PA6 lacks such internal field-concentrating interfaces and therefore experiences a more uniform electric-field distribution, allowing it to maintain a longer lifetime under the same high-field and high-temperature conditions.

At lower electric fields (<70 kV/mm), significant differences emerged. The PA6/10 wt.% BTO nanocomposite consistently showed longer time to breakdown than neat PA6 at all temperatures. In the range 333–353 K, the PA6/10 wt.% BTO nanocomposite exhibits a lifetime enhancement of approximately 30–50%, which further increases to over 70% at 373 K under an applied electric field of 60 kV/mm. This enhancement may be attributed to the presence of well-dispersed nanoparticles that introduce deep and shallow interfacial traps [37–39], suppressing charge mobility [40,41], charge injection [27,33,42] and moderating the internal electric-field distribution [37,43], while void reduction at the polymer–particle interface [3] may further contribute to the improved performance. These interfacial trapping mechanisms delay the onset of space-charge-induced ageing processes. This interpretation is supported by the dielectric spectroscopy measurements reported in [26], which showed that the introduction of nanoparticles reduces charge-transport processes in PA6/BTO nanocomposites at 353 K, particularly for the 5 wt.% and 10 wt.% BTO formulations, thereby extending the lifetime. The improved performance at 10 wt.% BTO aligns with established theories of polymer nanocomposites, where moderate filler concentrations create a beneficial trap distribution that impedes charge transport and stabilises dielectric response.

The behaviour at very high filler loading (20 wt.% BTO) deviated from this trend. These samples exhibited shorter lifetimes than neat PA6. At 353 K, the reduction in lifetime

ranges from approximately 90% at 90 kV/mm to about 20% at 50 kV/mm. At 373 K, the reduction is more pronounced at higher electric fields (80–90 kV/mm), where the lifetime decreases by approximately 60–80%. This reduction can be attributed to nanoparticle agglomeration [27] and a change in interfacial bonding at high filler concentrations [28], which lead to the formation of localised defects [3], micro voids [44], and sharp field-enhancing regions. These microstructural imperfections accelerate charge injection [26], enhance local electric stress, and promote early degradation, thereby negating the beneficial effects of nanofiller addition.

The DMM modelling results further support and clarify these observations. For neat PA6 and PA6/10 wt.% BTO, the DMM fit was performed over three temperatures (333, 353, and 373 K) and across the full 50–90 kV/mm field range. The extracted parameters (H/k, C/k, and b) for both materials were similar. This confirms that the intrinsic thermally activated ageing mechanism remains unchanged by the addition of nanofillers. The activation enthalpy term H/k, which reflects the thermal energy barrier associated with molecular degradation [17], was higher for the 10 wt.% BTO composite than the neat PA6. Slight increases in the H/k value accompanied by a decrease in the C/k value for the 10 wt.% composite indicate modest improvements in thermal robustness, consistent with the experimental observation that the nanocomposite provides extended lifetime at low electric fields (<70 kV/mm), as shown in Table 2. In this regime, the PA6/10 wt.% BTO samples demonstrate an increase in lifetime of approximately 31% at 353 K, 46.8% at 333 K, and 70% at 373 K compared to neat PA6. The slight changes in C/k and b suggest subtle modifications to the field-induced degradation kinetics [17] introduced by interfacial charge trapping, but not a fundamental change in ageing mechanism.

When the DMM model was applied to nanofiller concentrations (1, 5, 10, and 20 wt.% BTO), using the 353 K and 373 K datasets, a clear concentration-dependent pattern emerged. While the activation enthalpy H/k remained consistent across all samples, confirming unchanged intrinsic thermal ageing mechanisms, the parameters C/k and b varied systematically with filler content. The 1–10 wt.% composites exhibited field-dependent behaviour comparable to neat PA6, indicating that moderate nanofiller loadings modify ageing primarily through interfacial charge trapping and improved field homogenisation. The 10 wt.% BTO composite was identified as being the most resistant to ageing of them all.

In contrast to the other materials, the 20 wt.% composite exhibited significantly higher C/k, indicating increased susceptibility to damage from the electric field. These changes reflect microstructural defects introduced by nanoparticle agglomeration. The slightly lower value of b compared to neat PA6 suggests that the local field generated by trapped charges under a given applied field is weaker, likely because the charge density is reduced as it becomes distributed across the nanoparticle agglomerate. This reduction is, however, more than compensated by the higher destabilisation of the polymer segment arrangement in the vicinity of the charged agglomerate reflected in a significantly higher value of C/k. In addition, a slightly reduced activation enthalpy indicates that the nanocomposite agglomerate slightly increased the flexibility of the neighbouring polymer segments, as evidenced by the dielectric spectroscopy measurements reported in [26]. The overall picture therefore becomes one in which the larger size of the charged nanocomposite centre has a strong destabilising electro-mechanical effect on neighbouring polymer segments, thus more rapidly forcing modifications to the local structure. This shift in DMM parameters aligns closely with the experimental lifetime behaviour, indicating that long-term ageing performance is governed by microstructural features and nanoparticle–polymer interfacial mechanisms affecting long-term ageing performance [45].

Overall, the combined experimental and modelling results reveal that BTO nanoparticles enhance the electro-thermal endurance of PA6 when applied at low-to-moderate

concentrations (1–10 wt.%) through charge trapping, field homogenisation, and suppression of space-charge effects. However, excessive filler content (≥20 wt.%) introduces structural heterogeneities that intensify local electrical and thermal stresses and thus accelerate failure. The strong agreement between experimental lifetimes and DMM parameters confirms that the DMM model not only reproduces lifetime trends accurately but also provides insight into the interplay between temperature, electric field, and microstructure.

6. Conclusions

The electro-thermal ageing experiments demonstrated that the incorporation of BTO nanoparticles enhances the lifetime of PA6 insulation at low-to-moderate electric-field strengths (<70 kV/mm). Of all the compositions, the PA6/10 wt.% BTO nanocomposite exhibited the longest time to breakdown, confirming that well-dispersed ceramic nanoparticles introduce interfacial traps that suppress charge transport, homogenise the internal electric field, and delay the onset of degradation. However, this enhancement reduces at elevated temperatures, particularly at 373 K, where thermally activated charge mobility accelerates degradation. At high filler loading (20 wt.% BTO), the lifetime decreased below that of neat PA6, which is attributed to nanoparticle agglomeration and associated polymer–nanoparticle interfacial defects that intensify local electric stress and promote premature breakdown.

The Dissado–Montanari–Mazzanti (DMM) model was applied to neat PA6 and PA6/10 wt.% BTO across three temperatures (333 K, 353 K, and 373 K). The extracted activation enthalpy values (H/k) for both materials were nearly identical, demonstrating that the intrinsic thermally activated ageing mechanism of PA6 is fundamentally unchanged by the addition of resistance to BTO nanofillers. Slight variations in the parameters determining the effect of the electric field (C/k and b) reflect subtle differences in charge-trapping behaviour and local field redistribution, consistent with the mild lifetime improvements observed experimentally for the 10 wt.% nanocomposite. Extending the DMM analysis to all filler concentrations (1–20 wt.%) revealed that low-to-moderate loadings (1–10 wt.%) maintain resistance to electro-thermal ageing, while excessive loading (20 wt.%) significantly increases field sensitivity and hence results in shorter life due to agglomeration-induced microstructural defects.

The results show that optimised nanofiller incorporation can significantly enhance the electro-thermal endurance of PA6 without changing the ageing mechanism. Moreover, the agreement between experimental lifetime data and DMM model predictions confirms that the DMM framework provides a robust and physically meaningful tool for interpreting long-term ageing in polymer–ceramic nanocomposites under combined electrical and thermal stress.

Author Contributions: Conceptualization, K.R., L.D. and N.C.; methodology, N.C.; validation, K.R. and N.C.; formal analysis, K.R. and N.C.; investigation, K.R. and S.D.; resources, N.T. and N.C.; data curation, K.R. and S.D.; writing—original draft preparation, K.R. and N.C.; writing—review and editing, N.T., N.C. and L.D.; visualization, K.R.; supervision, N.T., L.D. and N.C.; project administration, N.C.; funding acquisition, N.T., L.D. and N.C. All authors have read and agreed to the published version of the manuscript.

Funding: This research was funded by the DPI (Dutch Polymer Institute), project number 852.

Data Availability Statement: The original contributions and data analysed in the present study are fully incorporated within this article. Requests for additional information may be addressed to the corresponding author.

Acknowledgments: The authors wish to thank the DPI Netherlands for sponsoring the work, project #852 and Envalior (formerly known as DSM) for the sample preparation.

Conflicts of Interest: Author Keyvan Rasti and Sathyamoorthy Dhayalan were employed by the company Dutch Polymer Institute. The remaining authors declare that the research was conducted in the absence of any commercial or financial relationships that could be construed as a potential conflict of interest.

Abbreviations

The following abbreviations are used in this manuscript:

DMM	Dissado–Montanari–Mazzanti
ETA	Electro-Thermal Ageing
PA6	Polyamide-6
BTO	Barium Titanate ($BaTiO_3$)

References

1. Lahti, K.; Rytöluoto, I.; Niittymäki, M.; Saarimäki, E.; Paajanen, M. From Laboratory to Industrial Scale: Comparison of Short-and Long-Term Dielectric Performance of Silica-Polypropylene Capacitor Films. In Proceedings of the 2020 IEEE 3rd International Conference on Dielectrics (ICD), Valencia, Spain, 5–31 July 2020; pp. 661–664.
2. Gubanski, S.M. Insulating materials for next generations of HVAC and HVDC cables. In Proceedings of the 2016 IEEE International Conference on High Voltage Engineering and Application (ICHVE), Chengdu, China, 19–22 September 2016; pp. 1–6.
3. Riggs, B.C.; Adireddy, S.; Rehm, C.H.; Puli, V.S.; Elupula, R.; Chrisey, D.B. Polymer nanocomposites for energy storage applications. *Mater. Today Proc.* **2015**, *2*, 3853–3863. [CrossRef]
4. Wang, Z.; Ye, L.; Liu, Y. Electro-thermal damage of carbon fiber/epoxy composite laminate. *J. Reinf. Plast. Compos.* **2018**, *37*, 166–180. [CrossRef]
5. Liang, M.; Wong, K.L. Improving the long-term performance of composite insulators use nanocomposite: A review. *Energy Procedia* **2017**, *110*, 168–173. [CrossRef]
6. Chen, S.; Skordos, A.; Thakur, V.K. Functional nanocomposites for energy storage: Chemistry and new horizons. *Mater. Today Chem.* **2020**, *17*, 100304. [CrossRef]
7. Khan, K.; Tareen, A.K.; Aslam, M.; Mahmood, A.; Zhang, Y.; Ouyang, Z.; Guo, Z.; Zhang, H. Going green with batteries and supercapacitor: Two dimensional materials and their nanocomposites based energy storage applications. *Prog. Solid State Chem.* **2020**, *58*, 100254. [CrossRef]
8. Yang, C.; Wei, H.; Guan, L.; Guo, J.; Wang, Y.; Yan, X.; Zhang, X.; Wei, S.; Guo, Z. Polymer nanocomposites for energy storage, energy saving, and anticorrosion. *J. Mater. Chem. A* **2015**, *3*, 14929–14941. [CrossRef]
9. Li, W.; Chen, M.; Yang, Y.; Yuan, D.; Ren, Y.; Cai, X. Dielectric property of modified barium titanate/polyamide 11 nanocomposites with different surfactants. *J. Appl. Polym. Sci.* **2019**, *136*, 47447. [CrossRef]
10. Kumar, R.; Gupta, N. Tracking and surface degradation of barium titanate filled silicone rubber nanocomposites. In Proceedings of the 2015 IEEE conference on electrical insulation and dielectric phenomena (CEIDP), Ann Arbor, MI, USA, 18–21 October 2015; pp. 495–498.
11. Kohutiar, M.; Kakošová, L.; Krbata, M.; Janík, R.; Fekiač, J.J.; Breznická, A.; Eckert, M.; Mikuš, P.; Timárová, Ľ. Comprehensive review: Technological approaches, properties, and applications of pure and reinforced polyamide 6 (PA6) and polyamide 12 (PA12) composite materials. *Polymers* **2025**, *17*, 442. [CrossRef]
12. Fan, B.; Liu, F.; Yang, G.; Li, H.; Zhang, G.; Jiang, S.; Wang, Q. Dielectric materials for high-temperature capacitors. *IET Nanodielectrics* **2018**, *1*, 32–40. [CrossRef]
13. Dissado, L.A.; Fothergill, J.C. *Electrical Degradation and Breakdown in Polymers*; IET: London, UK, 1992; Volume 9.
14. Ritamäki, M.; Rytöluoto, I.; Lahti, K.; Vestberg, T.; Pasanen, S.; Flyktman, T. Large-area approach to evaluate DC electro-thermal ageing behavior of BOPP thin films for capacitor insulation systems. *IEEE Trans. Dielectr. Electr. Insul.* **2017**, *24*, 826–836. [CrossRef]
15. Preetha, P.; Thomas, M.J.; Ranjan, R. Electrothermal ageing of epoxy nanocomposites. *IEEE Trans. Dielectr. Electr. Insul.* **2013**, *19*, 2081–2089. [CrossRef]
16. Ajour, M.N.; Dissado, L.A.; Fothergill, J.C.; Norman, P. Dielectric spectroscopy of epoxy/glass composite materials. In Proceedings of the Annual Report Conference on Electrical Insulation and Dielectric Phenomena, Cancun, Mexico, 20–24 October 2002; pp. 438–441.
17. Dissado, L.; Mazzanti, G.; Montanari, G. Elemental strain and trapped space charge in thermoelectrical aging of insulating materials. Part 1: Elemental strain under thermo-electrical-mechanical stress. *IEEE Trans. Dielectr. Electr. Insul.* **2002**, *8*, 959–965. [CrossRef]

18. Montanari, G.C.; Seri, P.; Dissado, L. Aging mechanisms of polymeric materials under DC electrical stress: A new approach and similarities to mechanical aging. *IEEE Trans. Dielectr. Electr. Insul.* **2019**, *26*, 634–641. [CrossRef]
19. Dissado, L. Predicting electrical breakdown in polymeric insulators. From deterministic mechanisms to failure statistics. *IEEE Trans. Dielectr. Electr. Insul.* **2002**, *9*, 860–875. [CrossRef]
20. Mazzanti, G. Life and reliability models for high voltage DC extruded cables. *IEEE Electr. Insul. Mag.* **2017**, *33*, 42–52. [CrossRef]
21. Choudhary, M.; Shafiq, M.; Kiitam, I.; Hussain, A.; Palu, I.; Taklaja, P. A review of aging models for electrical insulation in power cables. *Energies* **2022**, *15*, 3408. [CrossRef]
22. Mazzanti, G. The practical use of the DMM model for life estimation of HVDC cables subjected to qualification load cycles. *IEEE Trans. Dielectr. Electr. Insul.* **2024**, *31*, 1899–1908. [CrossRef]
23. Zuo, Z.; Dissado, L.; Yao, C.; Chalashkanov, N.; Dodd, S.; Gao, Y. Emergent failure patterns at sub-critical fields in polymeric dielectrics. *J. Mater. Sci.* **2020**, *55*, 4748–4761. [CrossRef]
24. Zuo, Z.; Dissado, L.; Yao, C.; Chalashkanov, N.; Dodd, S.; Gao, Y. Modeling for life estimation of HVDC cable insulation based on small-size specimens. *IEEE Electr. Insul. Mag.* **2019**, *36*, 19–29. [CrossRef]
25. Dhayalan, S.; Rasti, K.; Chalashkanov, N.; Tucker, N.; Dissado, L.A. Investigation of Effect of Nano-filler Concentration on the Life Estimation of Polyamide-6 Nanocomposites. In Proceedings of the 2024 IEEE 5th International Conference on Dielectrics (ICD), Toulouse, France, 30 June–4 July 2024; pp. 1–4.
26. Rasti, K.; Dhayalan, S.; Chalashkanov, N.; Tucker, N.; Dissado, L. Effect of Nanofiller Concentration on the Breakdown Strength of Polyamide Nanocomposites. In Proceedings of the 2023 IEEE Conference on Electrical Insulation and Dielectric Phenomena (CEIDP), East Rutherford, NJ, USA, 15–19 October 2023; pp. 1–4.
27. Lau, K.; Vaughan, A.; Chen, G. Nanodielectrics: Opportunities and challenges. *IEEE Electr. Insul. Mag.* **2015**, *31*, 45–54. [CrossRef]
28. Tanaka, T.; Montanari, G.C.; Mulhaupt, R. Polymer nanocomposites as dielectrics and electrical insulation-perspectives for processing technologies, material characterization and future applications. *IEEE Trans. Dielectr. Electr. Insul.* **2004**, *11*, 763–784. [CrossRef]
29. Pleşa, I.; Noţingher, P.V.; Schlögl, S.; Sumereder, C.; Muhr, M. Properties of polymer composites used in high-voltage applications. *Polymers* **2016**, *8*, 173. [CrossRef]
30. Nelson, W. Analysis of accelerated life test data-Part I: The Arrhenius model and graphical methods. *IEEE Trans. Electr. Insul.* **2007**, *EI-6*, 165–181. [CrossRef]
31. Liang, B.; Lan, R.; Zang, Q.; Liu, Z.; Tian, L.; Wang, Z.; Li, G. Influence of thermal aging on dielectric properties of high voltage cable insulation layer. *Coatings* **2023**, *13*, 527. [CrossRef]
32. Anghelescu, L.; Handra, A.D.; Diaconu, B.M. Degradation Pathways of Electrical Cable Insulation: A Review of Aging Mechanisms and Fire Hazards. *Fire* **2025**, *8*, 397. [CrossRef]
33. Tan, D.Q. The search for enhanced dielectric strength of polymer-based dielectrics: A focused review on polymer nanocomposites. *J. Appl. Polym. Sci.* **2020**, *137*, 49379. [CrossRef]
34. Waser, R.; Baiatu, T.; Härdtl, K.H. Dc electrical degradation of perovskite-type titanates: II, single crystals. *J. Am. Ceram. Soc.* **1990**, *73*, 1654–1662. [CrossRef]
35. Waser, R.; Baiatu, T.; Härdtl, K.H. dc electrical degradation of perovskite-type titanates: I, ceramics. *J. Am. Ceram. Soc.* **1990**, *73*, 1645–1653. [CrossRef]
36. Payne, D. Concerning the physics of failure of barium titanate capacitors. In Proceedings of the 6th Annual Reliability Physics Symposium (IEEE), Los Angeles, CA, USA, 6–8 November 1967; pp. 257–264.
37. Nelson, J.; Hu, Y. Nanocomposite dielectrics—Properties and implications. *J. Phys. D Appl. Phys.* **2005**, *38*, 213. [CrossRef]
38. Gao, J.; Liu, L.; Zhang, G.; Lee, T.; Schachtely, U.; Kobayashi, H. Effect of nanostructured SiO_2 on charge capture performance and electrical ageing life of PP nanocomposites. *High Volt.* **2025**, *10*, 186–196. [CrossRef]
39. Kamarudin, S.; Lau, K.; Ahmad, N.; Ching, K.; Ghani, A.; Arifin, N. Dielectric Breakdown Performance of Nanostructured Polypropylene Blend. In Proceedings of the 2025 IEEE Conference on Electrical Insulation and Dielectric Phenomena (CEIDP), Manchester, UK, 14–17 September 2025; pp. 189–192.
40. Zhou, Y.; Peng, S.; Hu, J.; He, J. Polymeric insulation materials for HVDC cables: Development, challenges and future perspective. *IEEE Trans. Dielectr. Electr. Insul.* **2017**, *24*, 1308–1318. [CrossRef]
41. Zhou, Y.; Zhu, Y.; Yuan, C.; Li, Q.; Xu, X.; Serdyuk, Y.; Wang, Q.; He, J. Insight into space charge suppression by interfacial deep traps in polymer nanocomposites. *IEEE Trans. Dielectr. Electr. Insul.* **2022**, *29*, 2402–2404. [CrossRef]
42. Pandey, J.C.; Singh, M. Dielectric polymer nanocomposites: Past advances and future prospects in electrical insulation perspective. *SPE Polym.* **2021**, *2*, 236–256. [CrossRef]
43. Wang, W.; Min, D.; Li, S. Understanding the conduction and breakdown properties of polyethylene nanodielectrics: Effect of deep traps. *IEEE Trans. Dielectr. Electr. Insul.* **2016**, *23*, 564–572. [CrossRef]

44. Mansour, D.-E.A.; Abdel-Gawad, N.M.; El Dein, A.Z.; Ahmed, H.M.; Darwish, M.M.; Lehtonen, M. Recent advances in polymer nanocomposites based on polyethylene and polyvinylchloride for power cables. *Materials* **2020**, *14*, 66. [CrossRef] [PubMed]
45. Rasti, K.; Dhayalan, S.; Mudbhatkal, A.; Tucker, N.; Dissado, L.; Chalashkanov, N. Effects of Electrothermal Ageing on the Structure of Polymer-Ceramic Nanocomposites. In Proceedings of the 2025 IEEE Conference on Electrical Insulation and Dielectric Phenomena (CEIDP), Manchester, UK, 14–17 September 2025; pp. 233–236.

Disclaimer/Publisher's Note: The statements, opinions and data contained in all publications are solely those of the individual author(s) and contributor(s) and not of MDPI and/or the editor(s). MDPI and/or the editor(s) disclaim responsibility for any injury to people or property resulting from any ideas, methods, instructions or products referred to in the content.